RESEARCH ARTICLE

Effect of Water Jet Peening on Fatigue Behavior of Inconel 718

Yixiao Li[1], Hanwen Li[1], Yu Nie[1], Siyu Zhou[1], Yawen Tan[1] and Yeran Gao[1,2,*]

[1] College of Intelligent Manufacturing, Qingdao Huanghai University, Qingdao 266520, China
[2] School of Mechanical and Automotive Engineering, Qingdao University of Technology, Qingdao 266520, China

Abstract

This study aims to elucidate the mechanisms governing residual stress formation and fatigue behavior in Inconel 718 subjected to water jet peening (WJP). A finite element model of the WJP process and a fatigue analysis model were developed using Abaqus and fe-safe, respectively. Particular attention was given to the residual stress, surface roughness, and fatigue life of WJP-treated Inconel 718. The results reveal that jet velocity exerts a dual effect on the strengthening response of Inconel 718. Jet velocity also strongly affects the fatigue resistance of specimens with thicknesses of 8 and 10 mm. However, once the jet velocity reaches 320 mm/s, the ability of WJP to induce compressive residual stress decreases, accompanied by deterioration of the surface morphology, which adversely affects fatigue behavior. Within the jet velocity range of 230–290 mm/s, the maximum compressive residual stress increases with increasing jet velocity. For specimens with thicknesses of 8, 10, and 12 mm, the differences in maximum compressive residual stress across this velocity range are approximately 170, 130, and 180 MPa, respectively. When the jet velocity is further increased to 320–350 mm/s, surface erosion reduces the effectiveness of compressive residual stress induction. The maximum compressive residual stress of the 8-mm-thick specimen falls slightly below that obtained at 290 mm/s, that of the 10-mm-thick specimen decreases by approximately 80 MPa from 320 to 350 mm/s, and that of the 12-mm-thick specimen treated at 320 mm/s is approximately 250 MPa lower than that obtained at 290 mm/s. The average surface roughness generally increases with increasing jet velocity. Surface cracks with depths of approximately 60–108 μm are observed in the 12-mm-thick specimens treated at 230–290 mm/s, whereas high-pressure WJP significantly suppresses subsequent crack propagation. The 8- and 10-mm-thick specimens exhibit superior fatigue resistance after WJP at 230–290 mm/s. Under an applied stress of 70 MPa, the maximum fatigue lives of the 8- and 10-mm-thick specimens reach 1,539,314 and 1,453,451 cycles, respectively. In contrast, the presence of surface cracks substantially reduces the fatigue lives of the 12-mm-thick specimens treated at 230–290 mm/s, for which the fatigue lives are 1,211,637, 1,111,250, and 1,296,931 cycles, respectively, under the same loading condition.

Submitted: 04 July 2026
Revised: 03 September 2026
Accepted: 07 September 2026
Published: 22 November 2026

Vol. 2, **No.** 1, 2026.
10.62762/JMDE.2026.467192

***Corresponding author:**
✉ Yeran Gao
gaoyeran2022@126.com

Citation
Li, Y., Li, H., Nie, Y., Zhou, S., Tan, Y., & Gao, Y. (2026). Effect of Water Jet Peening on Fatigue Behavior of Inconel 718. *Journal of Materials Durability and Engineering*, 2(1), 14–24.

© 2026 by the Authors. Published by Institute of Central Computation and Knowledge. This is an open access article under the CC BY license (https://creativecommons.org/licenses/by/4.0/).

Keywords: water jet peening, fatigue behavior, surface roughness, residual stress.

1 Introduction

The tailored composition of Inconel 718 provides an excellent combination of properties, including high strength, good creep resistance, and long fatigue life, making it widely used in hot-section components of aero-engines [1–3]. However, as aerospace vehicles are increasingly exposed to harsher service environments, improving the performance of structural components has become an urgent challenge. In particular, enhancing the fatigue resistance of Inconel 718 is crucial for ensuring the long-term service reliability of critical components. Surface strengthening techniques such as laser shock peening [4], shot peening [5], and ultrasonic surface rolling [6] can mitigate local stress concentrations and improve surface integrity. Nevertheless, these techniques suffer from relatively high cost, excessive noise, and limited accessibility, respectively. By contrast, water jet peening (WJP) offers several advantages, including environmental friendliness, low cost, and good accessibility. Water-jet-based treatments, such as submerged cavitating water jets and particle-assisted water jet peening, have been shown to effectively modify the surface morphology, roughness, and surface integrity of metallic materials [7, 8]. Consequently, WJP has attracted increasing research attention in recent years.

Arola et al. [9] applied high-pressure water jet peening to commercially pure titanium (cpTi) and Ti-6Al-4V alloy. Their results showed that substantial compressive residual stresses were induced, whereas the surface roughness of the target materials did not change significantly after treatment. These findings demonstrated the feasibility of high-pressure water jet peening for both cpTi and Ti alloys and suggested its potential as a surface strengthening technique for components with stringent surface-finish requirements. Sadasivam et al. [10] performed a parametric evaluation of abrasive water jet peening (AWJP) conducted on metallic specimens subjected to tensile elastic prestress. They showed that AWJP with elastic prestress could introduce substantial compressive residual stresses, although the treated surfaces exhibited a markedly rougher texture. Mahmoudi et al. [11] numerically and experimentally investigated the effects of water jet peening on the residual stress, surface roughness, and fatigue life of 7020 aluminum alloy. The results showed that water jet peening effectively improved the fatigue life of the alloy, which was strongly dependent on surface roughness. At high roughness levels, fatigue life decreased despite the introduction of substantial compressive residual stresses. Azhari et al. [12] investigated multiple-pass water jet peening of AISI 304 austenitic stainless steel. After 2, 4, and 6 peening passes, maximum compressive residual stresses of approximately 233.5, 260.1, and 405 MPa, respectively, were generated. Subsequent fatigue testing revealed that the fatigue limit of the peened specimens was lower than that of the untreated material. The authors attributed this behavior to the detrimental effects of increased surface roughness and the associated notch effect, which outweighed the beneficial contribution of the hardened surface layer. This study provided useful insight into fatigue performance evaluation after water jet peening and introduced multiple-pass peening as an alternative strengthening strategy. Yao et al. [13] employed submerged abrasive water jet peening to strengthen TA19 titanium alloy. The treated specimens exhibited substantial compressive residual stresses and a surface roughness of approximately 0.363 μm. Stress-controlled high-cycle fatigue (HCF) tests further showed that the HCF life could be increased by up to 2.72 times. This work broadened the processing strategies for water jet peening and provided a promising approach for simultaneously improving the surface integrity and fatigue performance of TA19 titanium alloy. Chakkravarthy et al. [14] investigated the hot-corrosion behavior of untreated and abrasive-water-jet-peened Ti-6Al-4V specimens. The hot-corrosion rate of the untreated surface was approximately 2.5 times that of the peened surface. The enhanced hot-corrosion resistance after peening was attributed to the compressive residual stress generated at the surface, which hindered chloride diffusion into the material. This study provided further insight into the potential applications of water jet peening and its role in improving surface-related performance.

Although increasing attention has been devoted to the fatigue performance of materials subjected to water jet peening, most previous studies have been conducted experimentally. More recently, Zhang et al. [15] combined numerical simulation and experiments to investigate the water jet impact damage mechanism and the dynamic penetration energy absorption of 2A12 aluminum alloy, revealing the deformation and damage response of the target material under water jet impact. This work provided

a new approach for evaluating the response of materials subjected to water jet impact. Zhang et al. [16] further clarified the influence mechanism of water jet peening on the fatigue crack growth behavior of 7075 aluminum alloy, demonstrating the close relationship between WJP-induced surface modification and fatigue performance. In the present study, a numerical model of water jet peening is established for Inconel 718 to systematically investigate the effects of different water jet peening parameters on the alloy and the fatigue behavior of the peened specimens. The results are expected to provide useful data and technical guidance for the fatigue-resistant design of Inconel 718 components.

2 Model Development for Water Jet Peening and Fatigue Performance Evaluation

A numerical model of water jet peening for Inconel 718 was developed using Abaqus, while the fatigue life of the peened specimens was evaluated using the fatigue durability analysis software fe-safe.

Figure 1(a) illustrates the numerical model established for water jet peening of Inconel 718. The model was constructed using the coupled Eulerian–Lagrangian (CEL) approach, in which the water domain was defined as an Eulerian body and the water jet directly impinged on the upper surface of the Inconel 718 specimen. The specimen geometry and dimensions are shown in Figure 1(b). The bottom surface of the specimen was fully constrained, and temperature–displacement coupled elements were adopted. The specimen mesh contained a total of 629,084 elements. The specimens were peened at different water jet velocities.

Fatigue damage in structural materials subjected to cyclic loading is a cumulative process. Each loading cycle contributes a certain amount of damage, and localized fatigue damage or fracture may occur once the accumulated damage reaches a critical level. Figure 1(c) shows the uniaxial tensile model of the water-jet-peened Inconel 718 specimen, with one end fixed and the opposite end subjected to tensile loading. The loading information and fatigue parameters were then imported into fe-safe to evaluate the fatigue life of Inconel 718 under different fatigue conditions. Water jet peening simulations and subsequent fatigue analyses were conducted according to the test matrix listed in Table 1.

The material behavior of Inconel 718 was described using the Johnson–Cook constitutive model, which

Table 1. Simulation scheme.

Water jet velocity (mm/s)	Specimen thickness (mm)	Applied stress (MPa)
230	8, 10, 12	70, 100
260	8, 10, 12	70, 100
290	8, 10, 12	70, 100
320	8, 10, 12	70, 100
350	8, 10, 12	70, 100

can be expressed as:

$$\sigma = (A + B\varepsilon^n)\left[1 + C\ln\left(\frac{\dot{\varepsilon}}{\dot{\varepsilon}_0}\right)\right]\left[1 - \left(\frac{T - T_0}{T_m - T_0}\right)^m\right] \quad (1)$$

where σ is the equivalent stress; A is the yield strength; B is the hardening modulus; ε is the equivalent plastic strain; n is the strain-hardening exponent; C is the strain-rate sensitivity coefficient; $\dot{\varepsilon}$ is the strain rate; $\dot{\varepsilon}_0$ is the reference strain rate; T is the instantaneous (current) temperature; T_0 is the reference temperature, which was set to 25 °C in the simulation; T_m is the melting temperature of the material; and m is the thermal softening exponent. The corresponding material parameters are listed in Table 2.

Table 2. Johnson–Cook constitutive parameters for Inconel 718.

Material	A/MPa	B/MPa	C	n	m	T_m/°C	T_0/°C
Inconel 718	435	278.94	0.019	0.96	0.34	620	25

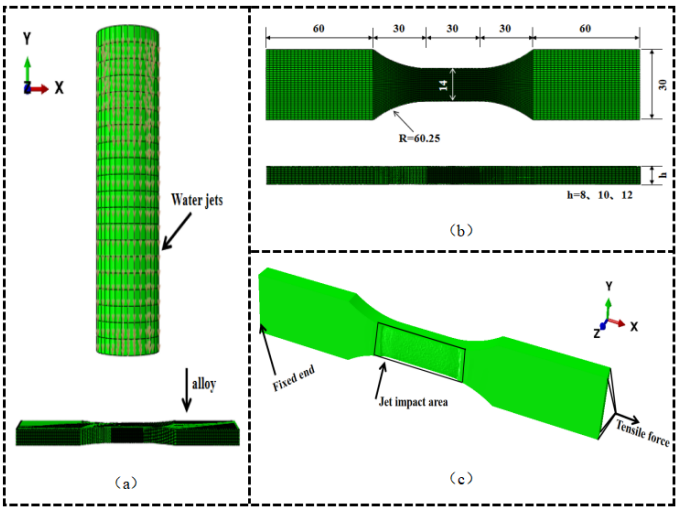


Figure 1. Numerical models used in this study: (a) water jet peening model, (b) specimen geometry and dimensions, and (c) uniaxial tensile model.

3 Simulation Results and Discussion

3.1 Residual Stress Analysis

For the 8-mm-thick specimen, the magnitude of the surface compressive residual stress within the peened region gradually increases from the center toward the edge of the water jet impact zone. Notably, changes in residual stress are also observed in regions not directly subjected to water jet peening. This behavior can be attributed to the interaction and superposition of stresses generated by successive water jet impacts. In the central region, multidirectional constraint imposed by the surrounding material produces a greater reaction force, thereby limiting the magnitude of the compressive residual stress. By contrast, regions outside the directly peened area are indirectly affected by the overflow of the water jet and consequently exhibit measurable changes in residual stress. As shown in Figure 2(f), the through-depth residual stress profiles of all specimens exhibit a characteristic spoon-shaped distribution, with the compressive residual stress magnitude initially increasing and then decreasing with depth. At a water jet velocity of 230 mm/s, the surface compressive residual stress is approximately 95 MPa. When the velocity increases to 290 mm/s, the surface compressive residual stress reaches its maximum value, increasing by approximately 82 MPa. Over the velocity range of 230–290 mm/s, the maximum compressive residual stress increases with increasing water jet velocity. At 290 mm/s, the maximum compressive residual stress reaches approximately 1420 MPa, which is about 170 MPa higher than that obtained at 230 mm/s. However, the depth corresponding to the maximum compressive residual stress remains nearly unchanged at approximately 67 μm. This behavior is attributed to the increase in dynamic pressure with increasing water jet velocity, which promotes more severe plastic deformation of the near-surface layer and thereby contributes to the development of higher compressive residual stresses. This is consistent with previous observations that water jet surface treatment introduces compressive residual stresses into the near-surface layer of metallic materials [9]. For specimens treated at water jet velocities of 320 and 350 mm/s, the surface compressive residual stresses are approximately 97 and 99 MPa, respectively. With increasing depth, however, shallow tensile residual stress regions appear at depths of approximately 2 and 17 μm, respectively. The corresponding maximum compressive residual stresses are approximately 1392 and 1401 MPa, occurring at depths of approximately 103 and 115 μm, respectively. Although the maximum compressive residual stress increases slightly with water jet velocity, the overall effectiveness of compressive residual stress induction remains relatively poor. This behavior is mainly attributed to the progressive erosion of the target surface at higher jet velocities. When the water jet velocity reaches 320–350 mm/s, a certain thickness of the surface layer is removed by erosion, resulting in partial removal of the compressive residual stress layer.

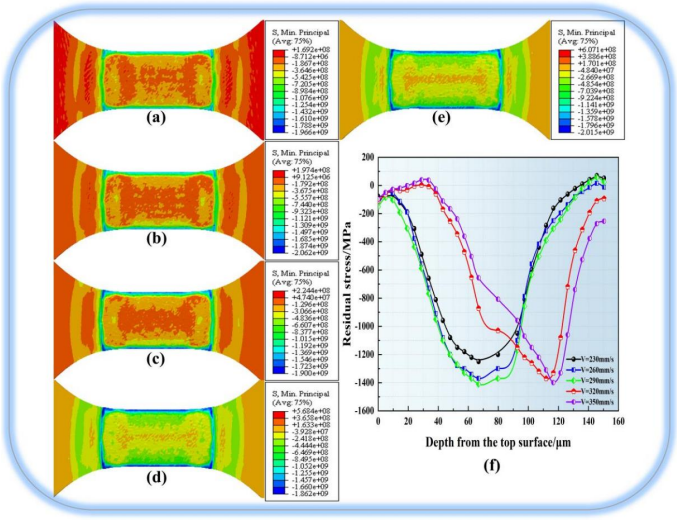


Figure 2. Residual stress distributions in the 8-mm-thick specimen after water jet peening at different jet velocities: (a) 230 mm/s, (b) 260 mm/s, (c) 290 mm/s, (d) 320 mm/s, (e) 350 mm/s, and (f) through-depth residual stress distribution.

The residual stress distribution and the corresponding through-depth residual stress profile of the 10-mm-thick specimen after water jet peening are shown in Figure 3. As shown in Figure 3(a–e), the peak compressive stress in the residual stress contours increases with increasing water jet velocity, and the value at 350 mm/s is approximately 1.20 times that obtained at 230 mm/s. As shown in Figure 3(f), the through-depth residual stress distribution of the 10-mm-thick specimen also exhibits a characteristic spoon-shaped profile after water jet peening. As the water jet velocity increases from 230 to 320 mm/s, the surface compressive residual stress decreases with increasing jet velocity. At 230 mm/s, the surface compressive residual stress is approximately 205 MPa higher than that obtained at 320 mm/s. In contrast, both the maximum compressive residual stress and the depth at which it occurs increase with increasing water jet velocity. At 320 mm/s, the maximum compressive residual stress is approximately 208 MPa higher than

that obtained at 230 mm/s. This behavior may be associated with the difference in surface integrity between the near-surface layer and the interior of Inconel 718 after water jet processing. Previous studies have shown that water jet processing markedly alters the surface integrity of Inconel 718, including its surface topography and near-surface residual stress state, and thereby affects its fatigue behavior [17, 18]. As the jet velocity increases, the near-surface layer directly exposed to the jet suffers more severe surface damage, which limits the surface compressive residual stress, whereas the subsurface material undergoes more extensive plastic deformation. In addition, increasing the water jet velocity raises the dynamic pressure acting on the target surface. For jet-peened Ti-6Al-4V, such intensified impact has been reported to promote severe plastic deformation and microstructural changes in the near-surface layer, which strengthen the induced compressive residual stress [19]. A similar mechanism is expected to enhance the development of compressive residual stress in the present specimens. After treatment at 350 mm/s, the maximum compressive residual stress decreases by approximately 80 MPa. Meanwhile, the depth corresponding to the maximum compressive residual stress increases by approximately 9 μm, whereas the depth at which the residual stress changes from compressive to tensile is the smallest among the investigated jet velocities, at approximately 180 μm. This behavior is attributed to the removal of a certain thickness of the surface layer by erosion under the high-velocity water jet. Such erosion removes part of the compressive residual stress layer and consequently reduces its overall depth. As discussed in the following section, the specimen treated at 350 mm/s also exhibits relatively high surface roughness, which further weakens the effectiveness of compressive residual stress induction.

For the 12-mm-thick specimen, as shown in Figure 4(a–e), distinct irregular regions of residual stress variation appear on the specimen surface after water jet peening at jet velocities of 230–290 mm/s. This behavior is mainly attributed to the formation of small surface cracks at these locations, which causes pronounced local changes in the residual stress distribution. As shown in Figure 4(f), over the jet velocity range of 230–290 mm/s, the surface compressive residual stress exhibits a negative correlation with jet velocity. After peening at 290 mm/s, a tensile residual stress of approximately 4 MPa appears on the specimen surface, whereas a

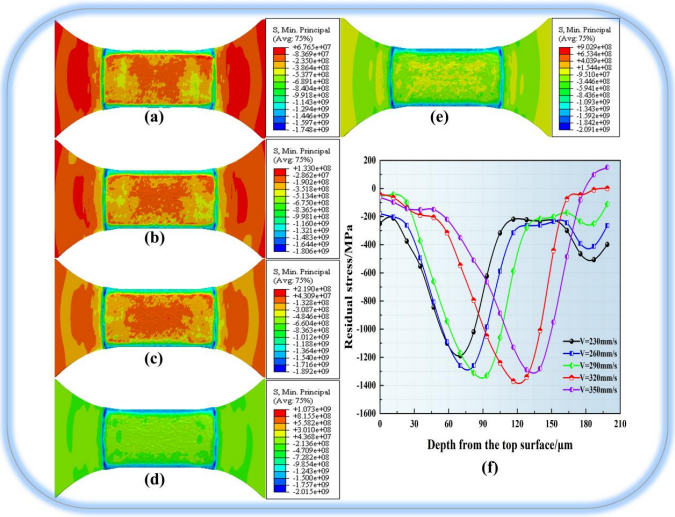


Figure 3. Residual stress distributions in the 10-mm-thick specimen after water jet peening at different jet velocities: (a) 230 mm/s, (b) 260 mm/s, (c) 290 mm/s, (d) 320 mm/s, (e) 350 mm/s, and (f) through-depth residual stress distribution.

compressive residual stress of approximately 50 MPa is observed at 230 mm/s. This behavior can be attributed to the unintended surface damage introduced during water jet peening. Kim et al. [20] showed that localized surface microcracking in shot-peened medium-carbon steel leads to the redistribution and relaxation of near-surface residual stress. Similarly, the surface damage formed here relaxes the near-surface compressive residual stress, causing the surface compressive residual stress to decrease with increasing jet velocity. In contrast, the maximum compressive residual stress increases with increasing jet velocity. After peening at 230 mm/s, the maximum compressive residual stress is approximately 1124 MPa and increases to approximately 1304 MPa when the jet velocity reaches 290 mm/s. Meanwhile, the depth corresponding to the maximum compressive residual stress also increases with jet velocity. At jet velocities of 230, 260, and 290 mm/s, the depths of the maximum compressive residual stress are approximately 90, 118, and 130 μm, respectively. This behavior can be attributed to the fact that compressive residual stress can still develop beneath the damaged surface. As the jet velocity increases, a more pronounced compressive residual stress field is induced, while the unintended damage extends deeper into the subsurface because of the disruption of the near-surface compressive residual stress layer. When the jet velocity is further increased to 320 and 350 mm/s, the maximum compressive residual stresses reach the lowest and highest levels among the five investigated

conditions, respectively, with corresponding values of approximately 1054 and 1364 MPa. Among the five jet velocities investigated, the compressive residual stress extends to the shallowest depth in the specimen treated at 320 mm/s, followed by that treated at 350 mm/s, with corresponding depths of approximately 205 and 230 μm, respectively.

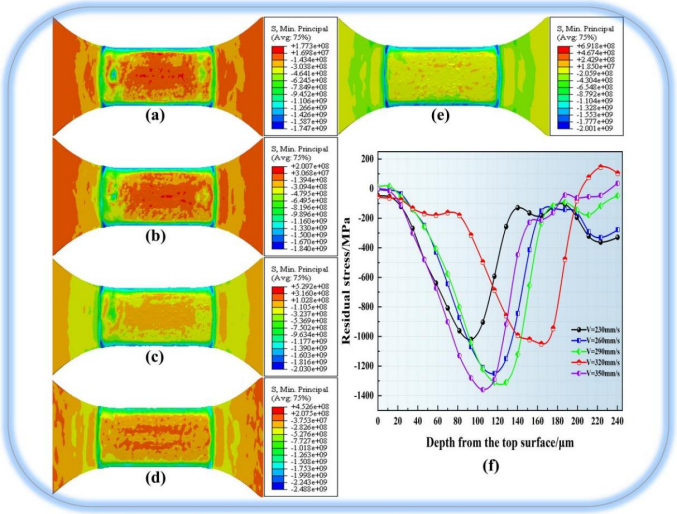


Figure 4. Residual stress distributions in the 12-mm-thick specimen after water jet peening at different jet velocities: (a) 230 mm/s, (b) 260 mm/s, (c) 290 mm/s, (d) 320 mm/s, (e) 350 mm/s, and (f) through-depth residual stress distribution.

3.2 Surface Roughness Analysis

Surface roughness and surface morphology are important indicators of surface integrity and play a critical role in the service life of the specimen. The surface profile within the water-jet-peened region was extracted from the vertical displacement (U2) of the surface nodes, and the average surface roughness (R_a) was calculated from this profile. As shown in Figure 5, fluctuations are observed in the profiles within the peened region, with particularly pronounced variations near the edges of the water jet impact zone. This behavior can be attributed to the spatial distribution of the jet impact. The central peened region is subjected to a relatively high density of water jet impacts, resulting in comparatively uniform plastic deformation. By contrast, the edges of the impact zone are subjected to jet loading predominantly from one side, resulting in a lower effective impact density than that in the central peened region. In addition, disturbances associated with the water jet promote local relaxation near the edges, leading to the formation of surface depressions, which are detrimental to fatigue life. As shown in Figure 5(a) and (b), the average surface roughness within the peened region generally increases with increasing water jet velocity. For the 8-mm-thick specimen treated at 350 mm/s, the maximum profile height at the edge reaches approximately 19.6 μm. The difference relative to the specimen treated at 230 mm/s is approximately 12.8 μm, while the difference in the average surface roughness within the peened region is approximately 4.20 μm. For the 10-mm-thick specimen, the difference in the maximum profile height at the edge between the specimens treated at 350 and 230 mm/s is approximately 14.5 μm, whereas the corresponding difference in the average surface roughness within the peened region is approximately 5.32 μm. This behavior is attributed to the increase in dynamic pressure acting on the target with increasing jet velocity, which induces more pronounced plastic deformation of the specimen surface. As shown in Figure 5(c), for the 12-mm-thick specimen treated at jet velocities of 230–290 mm/s, the average surface roughness initially increases and then decreases with increasing jet velocity. Pronounced peaks are observed in the surface profile within the peened region, corresponding to local deformation depths of approximately 78, 108, and 60 μm, respectively. These local deformations are associated with surface cracking and deterioration of the surface condition. The reduction in peak magnitude at higher jet velocity is attributed to the removal of surface defects by the high-pressure water jet. For submerged micro-abrasive water jet peening of TA19 titanium alloy, the treatment has been shown to induce severe plastic deformation, surface grain refinement, and substantial compressive residual stress, which suppress fatigue crack initiation and propagation [13]. The highest average surface roughness is observed in the specimen treated at 350 mm/s, reaching approximately 13.18 μm, indicating pronounced erosion within the water-jet-peened region.

3.3 Fatigue Life Analysis

The von Mises stress contours of the 8-mm-thick specimen under static tensile loading are shown in Figure 6. Tensile stresses of 70 and 100 MPa were applied to the free end of the specimen, with the opposite end fixed, as shown in Figure 1(c). After loading, relatively low stresses are observed at both ends of the specimen, whereas higher stresses develop in the central region, which represents the critical region for failure. The most critical location is situated at the edge of the water-jet-peened region. Under the same tensile load, the surface stress levels differ among specimens treated at different

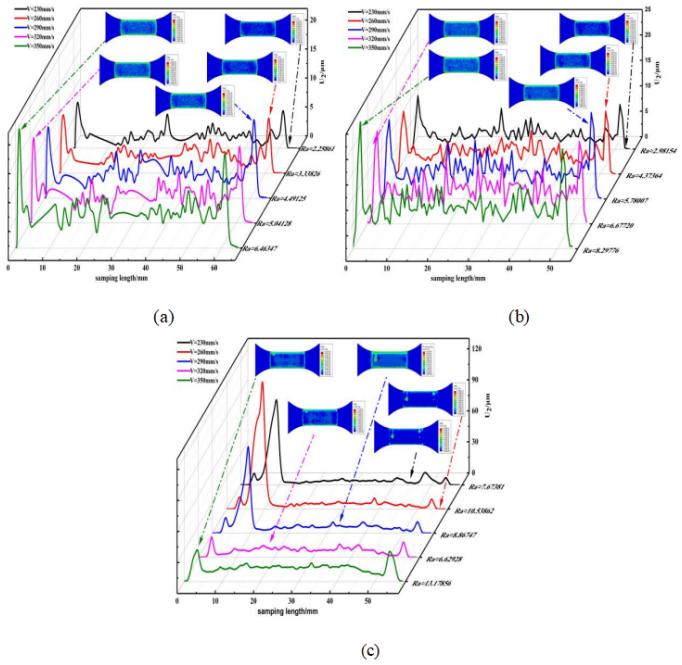


Figure 5. Surface roughness of specimens with different thicknesses after water jet peening: (a) 8 mm, (b) 10 mm, and (c) 12 mm.

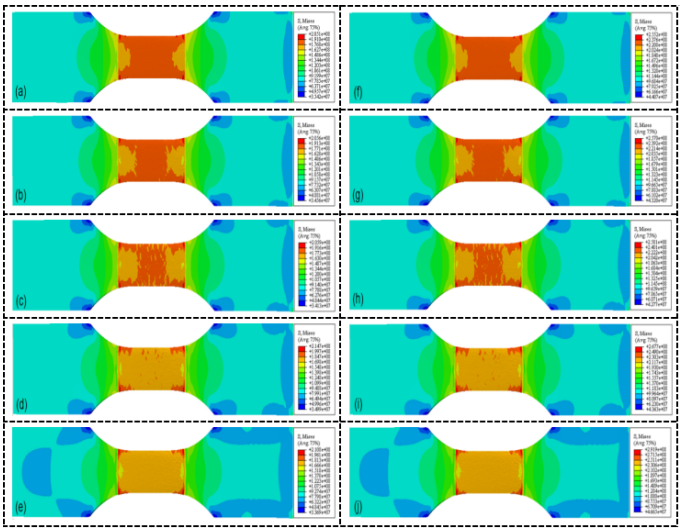


Figure 6. von Mises stress contours of the 8-mm-thick specimens treated at different water jet velocities under tensile loading: (a) 230 mm/s–70 MPa, (b) 260 mm/s–70 MPa, (c) 290 mm/s–70 MPa, (d) 320 mm/s–70 MPa, (e) 350 mm/s–70 MPa, (f) 230 mm/s–100 MPa, (g) 260 mm/s–100 MPa, (h) 290 mm/s–100 MPa, (i) 320 mm/s–100 MPa, and (j) 350 mm/s–100 MPa.

water jet velocities. Under an applied tensile stress of 70 MPa, the stresses in specimens peened at 230–290 mm/s are nearly identical, at approximately 205 MPa. For specimens treated at 320 and 350 mm/s, the corresponding stresses are approximately 215 and 210 MPa, respectively. This behavior is closely related to the combined effects of the compressive residual stress and surface roughness induced by water jet peening. When the jet velocity reaches 320–350 mm/s, the increase in compressive residual stress is relatively limited compared with that obtained at lower jet velocities, whereas the surface roughness increases markedly. Consequently, the load-bearing capacity of the specimen decreases under the same tensile loading condition, resulting in higher local stresses. When the applied tensile stress is increased to 100 MPa, the stress generated in the specimen shows a positive correlation with water jet velocity. The specimen peened at 350 mm/s exhibits a maximum stress of approximately 292 MPa under the 100 MPa tensile load, whereas the specimen treated at 230 mm/s shows a maximum stress of approximately 255 MPa under the same loading condition. The fatigue-life results of the 8-mm-thick specimens are shown in Figure 7. Numerical fatigue evaluation has been used to identify the critical high-cycle fatigue locations of nickel-based alloy components, such as Alloy 690TT steam generator tubes [21]. Accordingly, the red regions, which correspond to areas with relatively low predicted fatigue life, represent the locations most susceptible to fatigue failure. Under a tensile stress of 70 MPa, the numbers of cycles to failure for specimens peened at jet velocities of 230, 260, 290, 320, and 350 mm/s are 1,162,680, 1,539,314, 993,784, 697,246, and 802,507 cycles, respectively. Under a tensile stress of 100 MPa, the corresponding fatigue lives are 190,822, 253,991, 156,716, 118,740, and 127,074 cycles, respectively. Among the investigated conditions, the specimen treated at 260 mm/s exhibits the best fatigue performance, whereas the specimen treated at 320 mm/s exhibits the poorest fatigue resistance in this group. This difference can be attributed to the combined effects of surface roughness and compressive residual stress. The specimen peened at 260 mm/s exhibits a more favorable surface roughness level, while the induced compressive residual stress provides effective resistance to deformation. By contrast, the specimen treated at 320 mm/s exhibits a marked increase in surface roughness, which is detrimental to fatigue life. During fatigue loading, the near-surface compressive residual stress induced by peening can be redistributed and gradually relaxed, particularly where surface defects are present [20]. Specimens with poorer surface roughness undergo greater release of compressive residual stress during deformation, resulting in fewer cycles to fracture.

The von Mises stress contours of the 10-mm-thick

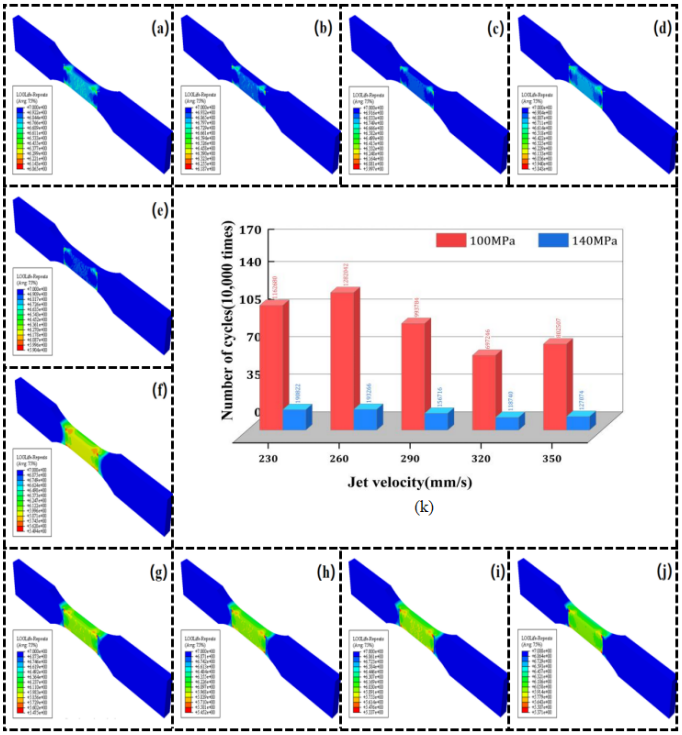


Figure 7. Fatigue lives of the 8-mm-thick specimens treated at different water jet velocities under tensile loading: (a) 230 mm/s–70 MPa, (b) 260 mm/s–70 MPa, (c) 290 mm/s–70 MPa, (d) 320 mm/s–70 MPa, (e) 350 mm/s–70 MPa, (f) 230 mm/s–100 MPa, (g) 260 mm/s–100 MPa, (h) 290 mm/s–100 MPa, (i) 320 mm/s–100 MPa, (j) 350 mm/s–100 MPa, and (k) number of cycles to failure.

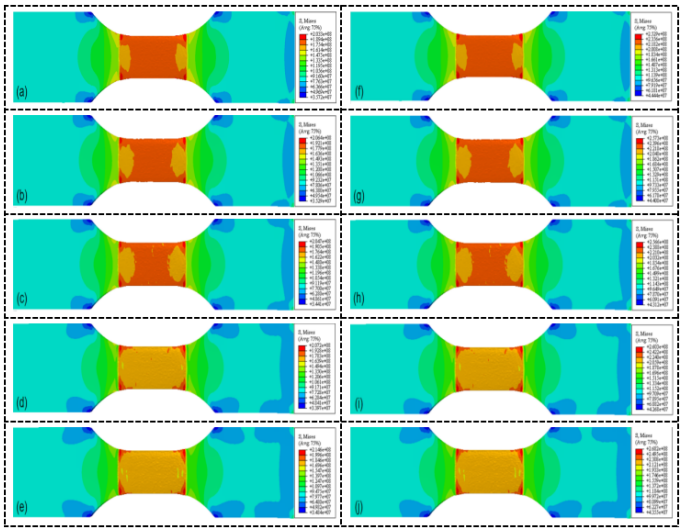


Figure 8. von Mises stress contours of the 10-mm-thick specimens treated at different water jet velocities under tensile loading: (a) 230 mm/s–70 MPa, (b) 260 mm/s–70 MPa, (c) 290 mm/s–70 MPa, (d) 320 mm/s–70 MPa, (e) 350 mm/s–70 MPa, (f) 230 mm/s–100 MPa, (g) 260 mm/s–100 MPa, (h) 290 mm/s–100 MPa, (i) 320 mm/s–100 MPa, and (j) 350 mm/s–100 MPa.

specimens under static tensile loading are shown in Figure 8. The fatigue-life results of the 10-mm-thick specimens are shown in Figure 9. The most critical region remains located at the edge of the water-jet-peened zone. Although high-pressure water jet peening induces substantial compressive residual stress in this region, the edge depressions adversely affect fatigue life because the associated stress concentration promotes fatigue crack initiation. Under an applied tensile stress of 70 MPa, the numbers of cycles to failure for specimens treated at jet velocities of 230, 260, 290, 320, and 350 mm/s are 1,450,582, 1,344,427, 1,453,451, 1,282,042, and 794,318 cycles, respectively. When the applied tensile stress is increased to 100 MPa, the fatigue lives decrease markedly to 233,216, 213,253, 220,560, 193,266, and 131,297 cycles, respectively.

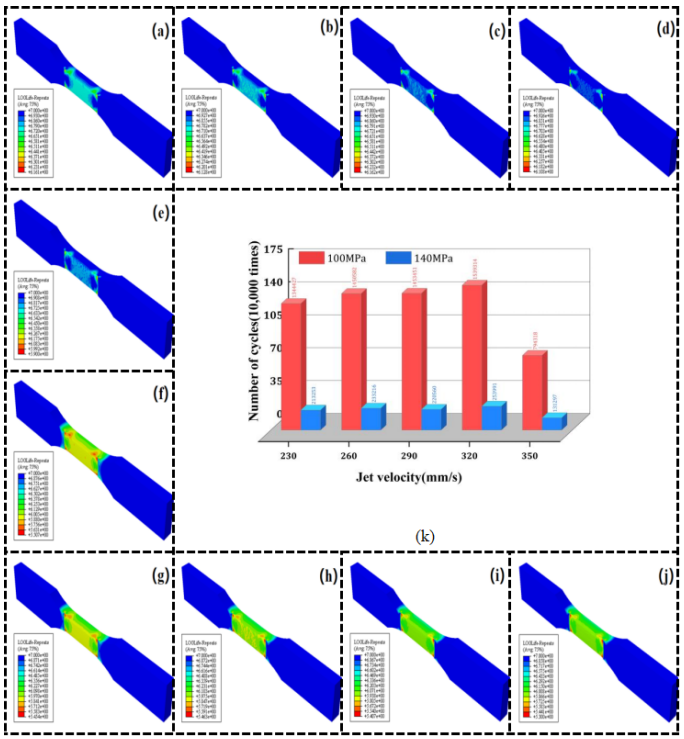


Figure 9. Fatigue lives of the 10-mm-thick specimens treated at different water jet velocities under tensile loading: (a) 230 mm/s–70 MPa, (b) 260 mm/s–70 MPa, (c) 290 mm/s–70 MPa, (d) 320 mm/s–70 MPa, (e) 350 mm/s–70 MPa, (f) 230 mm/s–100 MPa, (g) 260 mm/s–100 MPa, (h) 290 mm/s–100 MPa, (i) 320 mm/s–100 MPa, (j) 350 mm/s–100 MPa, and (k) number of cycles to failure.

Among the investigated conditions, the specimen peened at 350 mm/s exhibits the lowest number of cycles to failure. This behavior is mainly attributed to the pronounced deterioration of the surface morphology after high-pressure water jet peening

and the relatively poor effectiveness of compressive residual stress induction. Similar to the fatigue failure behavior of the 8-mm-thick specimens, greater release of compressive residual stress occurs during deformation, resulting in a lower fatigue life.

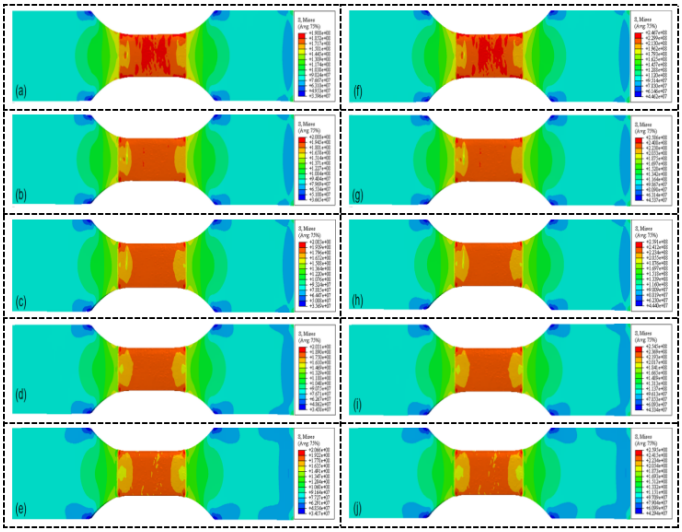


Figure 10. von Mises stress contours of the 12-mm-thick specimens treated at different water jet velocities under tensile loading: (a) 230 mm/s–70 MPa, (b) 260 mm/s–70 MPa, (c) 290 mm/s–70 MPa, (d) 320 mm/s–70 MPa, (e) 350 mm/s–70 MPa, (f) 230 mm/s–100 MPa, (g) 260 mm/s–100 MPa, (h) 290 mm/s–100 MPa, (i) 320 mm/s–100 MPa, and (j) 350 mm/s–100 MPa.

The von Mises stress contours of the 12-mm-thick specimens under static tensile loading are shown in Figure 10. Pronounced stress variations are observed in the vicinity of the cracks, although the stress magnitudes in these regions are lower than those in the other areas affected by the water jet. Under an applied tensile stress of 70 MPa, the specimen peened at 230 mm/s exhibits a maximum stress of approximately 198.8 MPa, whereas the specimens treated at 260 and 290 mm/s both exhibit maximum stresses of approximately 208 MPa. When the applied tensile stress is increased to 100 MPa, the specimen peened at 230 mm/s shows the lowest stress, approximately 246.7 MPa, while the specimens treated at 260 and 290 mm/s exhibit similar maximum stresses of approximately 259 MPa. As shown in Figure 11, under an applied tensile stress of 70 MPa, the numbers of fatigue cycles for specimens treated at jet velocities of 230, 260, 290, 320, and 350 mm/s are 1,211,637, 1,111,250, 1,296,931, 1,767,373, and 1,515,372 cycles, respectively. Under a tensile stress of 100 MPa, the corresponding numbers of fatigue cycles are 198,307, 190,429, 195,618, 283,715, and 229,325 cycles, respectively. For specimens peened at jet velocities of 230–290 mm/s, the number of fatigue cycles generally decreases with increasing crack depth, indicating that deeper surface cracks markedly reduce the fatigue life of the specimens.

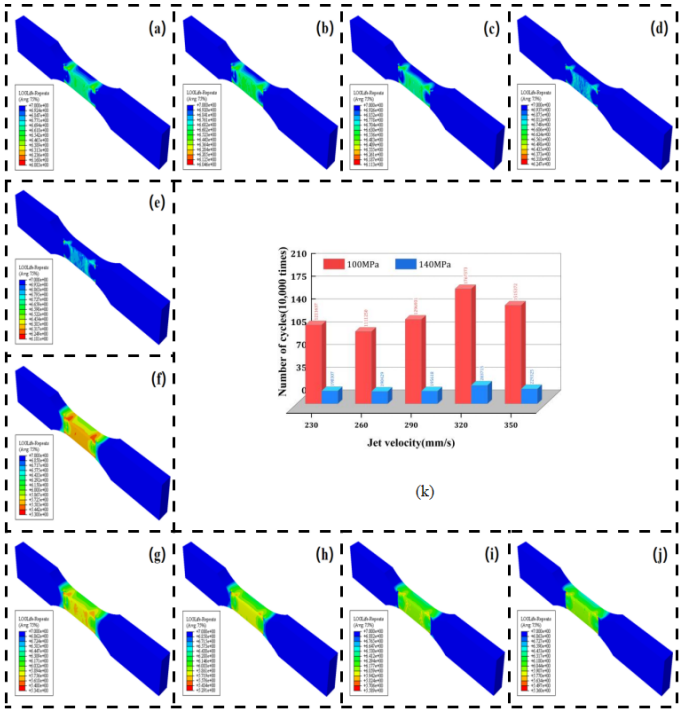


Figure 11. Fatigue lives of the 12-mm-thick specimens treated at different water jet velocities under tensile loading: (a) 230 mm/s–70 MPa, (b) 260 mm/s–70 MPa, (c) 290 mm/s–70 MPa, (d) 320 mm/s–70 MPa, (e) 350 mm/s–70 MPa, (f) 230 mm/s–100 MPa, (g) 260 mm/s–100 MPa, (h) 290 mm/s–100 MPa, (i) 320 mm/s–100 MPa, (j) 350 mm/s–100 MPa, and (k) number of cycles to failure.

4 Conclusions

This study investigated the strengthening effect of water jet peening on Inconel 718 and the resulting fatigue performance. A finite element model of water jet peening was established for Inconel 718, and the fatigue performance of the peened specimens was subsequently evaluated. Particular attention was given to the residual stress, surface roughness, and number of cycles under cyclic loading. The main conclusions are as follows:

(1) The residual stress state induced in Inconel 718 is strongly influenced by water jet velocity. Within the range of 230–290 mm/s, increasing the jet velocity promotes the development of compressive residual stress. Over this velocity range, the differences in maximum compressive residual stress for the 8-, 10-, and 12-mm-thick specimens are approximately 170,

130, and 180 MPa, respectively. However, when the water jet velocity increases to 320–350 mm/s, excessive jet velocity causes surface erosion, thereby reducing the effectiveness of compressive residual stress induction.

(2) The strengthening effect should be evaluated by considering both the induced compressive residual stress and the resulting surface roughness. The average surface roughness of the Inconel 718 specimens generally increases with increasing water jet velocity. Notably, pronounced plastic deformation develops near the edges of the water-jet-peened region, and surface cracking may also occur during peening. For the 12-mm-thick specimens treated at jet velocities of 230, 260, and 290 mm/s, the corresponding crack depths are approximately 78, 108, and 60 μm, respectively.

(3) The compressive residual stress induced by water jet peening contributes to improved fatigue performance, whereas increased surface roughness adversely affects fatigue life. Therefore, the final fatigue performance is governed by the combined effects of compressive residual stress and surface roughness. Among the conditions investigated, the thickness–jet velocity combinations that provide relatively favorable fatigue performance are 8 mm–260 mm/s, 10 mm–290 mm/s, and 12 mm–320 mm/s.

Data Availability Statement

Data will be made available on request.

Funding

This work was supported in part by the Natural Science Foundation of Shandong Province under Grant ZR2016EEP03; in part by the Applied Basic Research Program of Qingdao City under Grant 19-6-2-69-cg; and in part by the Shandong Qingchuang Science and Technology Project under Grant 2019KJB022.

Conflicts of Interest

The authors declare no conflicts of interest.

AI Use Statement

The authors declare that no generative AI was used in the preparation of this manuscript.

Ethical Approval and Consent to Participate

Not applicable.

References

[1] Zhang, D., Niu, W., Cao, X., & Liu, Z. (2015). Effect of standard heat treatment on the microstructure and mechanical properties of selective laser melting manufactured Inconel 718 superalloy. *Materials Science and Engineering: A, 644*, 32-40. [CrossRef]

[2] Tucho, W. M., Cuvillier, P., Sjolyst-Kverneland, A., & Hansen, V. (2017). Microstructure and hardness studies of Inconel 718 manufactured by selective laser melting before and after solution heat treatment. *Materials Science and Engineering: A, 689*, 220-232. [CrossRef]

[3] Thomas, A., El-Wahabi, M., Cabrera, J. M., & Prado, J. M. (2006). High temperature deformation of Inconel 718. *Journal of Materials Processing Technology, 177*(1-3), 469-472. [CrossRef]

[4] Chen, H., Ge, L., Liu, X., Tian, Z., Xu, B., & Hua, G. (2022). Effect of curvature of concave model on strengthening effect of 7050-T7451 aluminum alloy by laser shock. *Applied Physics A, 128*(8), 704. [CrossRef]

[5] Yin, F., Zhang, X., Chen, F., Hu, S., Ming, K., Zhao, J., ... & Wang, J. (2023). Understanding the microstructure refinement and mechanical strengthening of dual-phase high entropy alloy during ultrasonic shot peening. *Materials & Design, 227*, 111771. [CrossRef]

[6] Xu, X., Liu, D., Zhang, X., Liu, C., Liu, D., & Zhang, W. (2019). Influence of ultrasonic rolling on surface integrity and corrosion fatigue behavior of 7B50-T7751 aluminum alloy. *International Journal of Fatigue, 125*, 237-248. [CrossRef]

[7] Hutli, E., Nedeljkovic, M., & Bonyár, A. (2018). Controlled modification of the surface morphology and roughness of stainless steel 316 by a high speed submerged cavitating water jet. *Applied Surface Science, 458*, 293-304. [CrossRef]

[8] Zhang, P., Yue, X., Wang, P., & Zhai, Y. (2022). Influence of SiC pellets water jet peening on the surface integrity of 7075-T6 aluminum alloy. *Vacuum, 196*, 110760. [CrossRef]

[9] Arola, D., McCain, M. L., Kunaporn, S., & Ramulu, M. (2001). Waterjet and abrasive waterjet surface treatment of titanium: a comparison of surface texture and residual stress. *Wear, 249*(10-11), 943-950. [CrossRef]

[10] Sadasivam, B., Hizal, A., & Arola, D. (2009). Abrasive waterjet peening with elastic prestress: A parametric evaluation. *International Journal of Machine Tools and Manufacture, 49*(2), 134-141. [CrossRef]

[11] Mahmoudi, A. H., Jamali, A. M., Salahi, F., & Khajeian, A. (2021). Effects of water jet peening on residual stresses, roughness, and fatigue. *Surface Engineering, 37*(8), 972-981. [CrossRef]

[12] Azhari, A., Schindler, C., Godard, C., Gibmeier, J., & Kerscher, E. (2016). Effect of multiple passes treatment in waterjet peening on fatigue performance. *Applied Surface Science, 388*, 468-474. [CrossRef]

[13] Yao, S. L., Wang, G. Y., Yu, H., Wang, J., Li, K. S., Liu, S., ... & Tu, S. T. (2022). Influence of submerged micro-abrasive waterjet peening on surface integrity and fatigue performance of TA19 titanium alloy. *International Journal of Fatigue, 164*, 107076. [CrossRef]

[14] Chakkravarthy, V., Oliveira, J. P., Mahomed, A., Yu, N., Manojkumar, P., Lakshmanan, M., ... & Narayan, R. L. (2023). Effect of abrasive water jet peening on NaCl-induced hot corrosion behavior of Ti–6Al–4V. *Vacuum, 210*, 111872. [CrossRef]

[15] Zhang, P., Liu, Z., Yue, X., Wang, P., & Zhai, Y. (2022). Water jet impact damage mechanism and dynamic penetration energy absorption of 2A12 aluminum alloy. *Vacuum, 206*, 111532. [CrossRef]

[16] Zhang, P., Gao, Y., Zhang, J., Yue, X., Zhou, H., & Sun, Y. (2024). The influence mechanism of water jet peening on the fatigue crack growth behavior of 7075 aluminum alloy. *International Journal of Fatigue, 187*, 108429. [CrossRef]

[17] Rivero, A., Alberdi, A., Artaza, T., Mendia, L., & Lamikiz, A. (2018). Surface properties and fatigue failure analysis of alloy 718 surfaces milled by abrasive and plain waterjet. *The International Journal of Advanced Manufacturing Technology*, 94(5-8), 2929-2938. [CrossRef]

[18] Cano Salinas, L., Moussaoui, K., Hejjaji, A., Salem, M., Hor, A., & Zitoune, R. (2021). Influence of abrasive water jet parameters on the surface integrity of Inconel 718. *The International Journal of Advanced Manufacturing Technology*, 114(3-4), 997-1009. [CrossRef]

[19] Wan, L., Cai, J., Qian, Y., Wu, S., Kang, Y., & Li, D. (2024). Surface integrity and fatigue performance of Ti6Al4V alloy peened by sinking bead abrasive jet. *Journal of Materials Research and Technology*, 32, 3169-3180. [CrossRef]

[20] Kim, J. C., Cheong, S. K., & Noguchi, H. (2013). Evolution of residual stress redistribution associated with localized surface microcracking in shot-peened medium-carbon steel during fatigue test. *International Journal of Fatigue, 55*, 147-157. [CrossRef]

[21] Li, Z., Wang, X., Wang, J., Lu, Y., & Shoji, T. (2020). High cycle fatigue behavior and numerical evaluation of Alloy 690TT steam generator tube. *International Journal of Fatigue, 137*, 105662. [CrossRef]